Enabling Resilient Community Microgrids with Multiple Points of Common Coupling via a Rank-Based Model Predictive Control Framework

Brevann Nun[1], Muhammad Farooq Umar[2], Mohammad B. Shadmand[2]
[1]Department of Electrical & Computer Engineering, Kansas State University, Manhattan, KS, USA
[2]Department of Electrical & Computer Engineering, University of Illinois at Chicago, IL, USA
brevannn@ksu.edu, mumar6@uic.edu, shadmand@uic.edu

***Abstract*—This paper presents an adaptive rank-based model predictive control (MPC) scheme for voltage source converters (VSCs) operating in a low voltage, AC community microgrid with dynamically changing topology. The proposed framework enables a fully synchronized microgrid with the ability to connect multiple VSCs to the utility grid simultaneously through multiple points of common coupling (MPCC). Furthermore, the VSCs autonomously adjust their operational mode from grid-forming to grid-following and vice versa, attaining a higher margin of stability, robustness, and flexibility. The MPC framework features an adaptive ranking system that assigns operational modes of the VSCs, i.e. voltage control (grid-forming) or current control (grid-following). The MATLAB/Simulink simulated case studies validate the controller's functionality and flexibility while operating in changing microgrid configurations. A small-scale hardware testbed validates the practical implementation of the proposed controller.**

***Index Terms* – model predictive control, microgrids, multiple point of common coupling, grid synchronization, voltage source converters.**

I. Introduction

Recent advancements in renewable energy systems have led to the proliferation of distributed energy resources (DERs) on the grid. These resources, such as PV solar and wind energy harvesting plants, enable localized energy generation and storage that interface with an AC bus via VSCs. The community microgrid is an emerging technology with the potential to boost grid reliability by utilizing DERs to offer multiple modes of system operation, i.e. islanded or grid-connected mode [1-3] . The U.S. Department of Energy (DOE) defines microgrid as "a group of interconnected loads and distributed energy resources within clearly defined electrical boundaries that acts as a single controllable entity with respect to the grid. A microgrid can connect and disconnect from the grid to enable operation in both grid-connected or islanded mode" [4]. In a power electric dominated grid (PEDG) [3, 5], a microgrid can be considered as a grid cluster with the ability to either integrate with the rest of the utility grid via a single or multiple point of common coupling (MPCC) or operate in an islanded, standalone mode [1, 6]. It is this flexibility in operational mode which gives microgrid clusters (i.e. PEDG) superior robustness and reliability.

The concept of multiple points of common coupling has recently emerged as a feature of microgrids to further increase reliability by connecting to the utility grid at several points. Such topologies offer redundancy in the event of a disruption at the PCC node and generally increase the flexibility of system operators. However, these dynamic topologies present other challenges. An interconnected grid comprising dispersed utility coupling points implies bidirectional power flow rather than the traditional unidirectional feeder topology. Distributed controllers must offer operational compatibility at nodes with bidirectional flow. Further, every VSC throughout a MPCC-equipped network should be capable of adapting its operational mode to changing topologies or system-level objectives. These challenges must be satisfied while simultaneously maintaining at least one voltage-controlled VSC within an islanded microgrid to prevent opposing waveforms.

The limitations of controllers performing in such a microgrid topology are twofold: (i) existing VSC controllers are unable to cope with changing network topologies in a microgrid with MPCC, and (ii) the voltage of an islanded microgrid collapses if the grid-forming source is disconnected or interrupted intentionally/unintentionally [7]. Both limitations increase susceptibility to system faults, either on the grid's PCC or on the grid-forming VSC's point of connection. The solution to these problems lies in the implementation of a system that can adapt VSC modes of operation via seamless transitions, depending on the current system configuration.

Existing literature investigates control techniques for the smooth transition between grid-connected and islanded modes of a microgrid with a single PCC. The authors in [8] present a VSC controller that uses model predictive control (MPC) to seamlessly transition between grid-connected and islanded modes by adjusting the control variables' weight factors. The authors in [9] and [10] use distributed averaging to adapt droop-controlled VSCs to various islanded and grid-tied network topologies. Averaging mode droop controllers benefit from a sparse communication layer and can successfully operate in many, though not all, microgrid system configuration changes.

This paper proposes a rank-based MPC for distributed VSCs operating in a re-configurable microgrid with dynamic boundaries and MPCC. A ranking scheme is proposed that allows the identity of a system's grid-forming VSC to adapt autonomously, thus providing flexibility to the control structure of the network. The proposed rank-based MPC framework results in fully synchronized, re-configurable microgrids while enhancing grid resiliency for high renewable energy penetration. Furthermore, it allows islanded operation without the primary grid-forming source

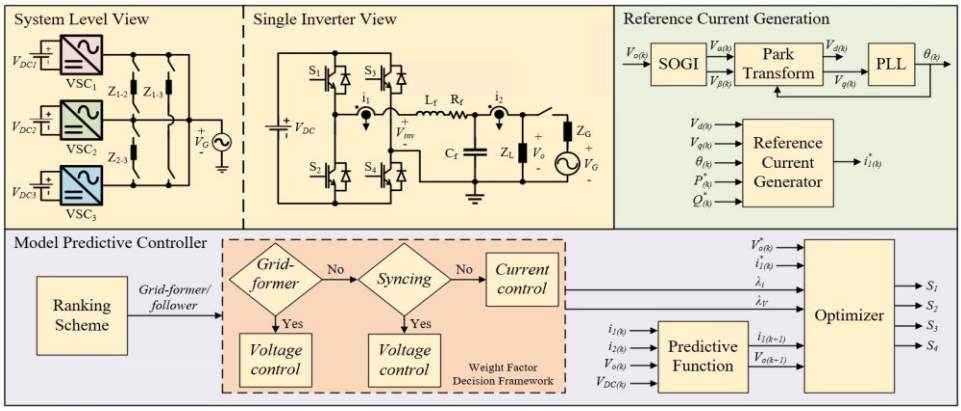

Fig. 1. Proposed system configuration

by delegating grid-forming functionality to another VSC, thereby guaranteeing exactly one voltage-controlled source at all times. These transitions are seamless and exhibit robust performance within a microgrid of dynamic configuration.

The design of the proposed controller leverages MPC that reduces the effort of tuning a controller, provides single loop design, and offers fast dynamic response [11-15]. Additionally, with MPC, the VSCs can operate seamlessly in two different modes, i.e. current-control, and voltage-control mode. The cost function of the MPC scheme contains parameters for voltage and current control, while respective weight factors ensure that only one parameter is selected at a time. The weight factors are provided by an adaptive ranking scheme that assigns ranks to each VSC depending on the existing system's configuration. The rank-based framework operates with use of a sparse communication layer that mirror's the physical topology of the system. Finally, the control structure ensures proper performance and reliable operation according to grid standards by limiting current spikes and voltage transients during grid-connecting or internal reconfiguration transitions.

The remainder of this paper is organized as follows: Section II describes the mathematical model of the predictive controller. Section III introduces the proposed rank-based control strategy. Simulation results are presented in Section IV while a brief hardware analysis is included in Section V. Finally, Section VI provides a summary and concluding remarks.

II. Proposed System Model

Fig. 1 shows system-level and single inverter views of the proposed configuration. Each VSC interfaces with its own local AC bus via an LC filter. The local buses of *n* VSCs are connected to one another by an interconnected microgrid and may tie directly to the utility grid via a PCC. In this paper, a single inverter is considered when evaluating the equivalent system model.

A. Mathematical Model

The discretized prediction method proposed in [16] for three-phase inverters with LCL filters is adapted to the single-phase, LC VSCs of the proposed microgrid. The grid current prediction can be determined from LC filter side KVL equation,

$$\frac{di_1}{dt} = \frac{1}{L_f}\left[v_{inv} - i_1 R_f - v_o\right] \tag{1}$$

$$\frac{dv_o}{dt} = \frac{1}{C_f}\left[i_1 - i_2\right] \tag{2}$$

where R_f, L_f, and C_f are the values of the discrete passive elements of the output filter. The state space representation of this continuous-time system is given by,

$$\frac{d}{dt}\begin{bmatrix} i_{1,k} \\ v_{o,k} \end{bmatrix} = A\begin{bmatrix} i_{1,k} \\ v_{o,k} \end{bmatrix} + B\begin{bmatrix} v_{inv,k} \\ i_{2,k} \end{bmatrix} \tag{3}$$

where system matrices A and B are defined as follows,

$$A = \begin{pmatrix} -\frac{R_f}{L_f} & -\frac{1}{L_f} \\ \frac{1}{C_f} & 0 \end{pmatrix}, \qquad B = \begin{pmatrix} \frac{1}{L_f} & 0 \\ 0 & -\frac{1}{C_f} \end{pmatrix}$$

This system is then discretized for time step T_s and solved for step-ahead estimations,

$$\begin{bmatrix} i_{1,k+1} \\ v_{o,k+1} \end{bmatrix} = A_d\begin{bmatrix} i_{1,k} \\ v_{o,k} \end{bmatrix} + B_d\begin{bmatrix} v_{inv,k} \\ i_{2,k} \end{bmatrix} \tag{4}$$

where matrices A_d and B_d are defined using their continuous counterparts as follows,

$$A_d = e^{AT_s}, \qquad B_d = A^{-1}\left(A_d - I\right)B$$

Finally, an estimation for the output current $i_{2,k+1}$ can be calculated by,

$$i_{2,k+1} = i_{1,k+1} - C\left(\frac{v_{o,k+1} - v_{o,k}}{T_s}\right) \tag{5}$$

B. Reference Current Generation

Fig. 1 shows second order generalized integrator (SOGI) paired with a Park transformation and phase lock loop (PLL) to generate the *dq* components, $v_{d,k}$ and $v_{q,k}$, and phase angle θ_k of the output voltage. Reference current $i^*_{2,k}$ for a current controlled VSC is given by,

$$\begin{aligned} i^*_{2,k} &= i^*_{d,k}\sin\theta_k + i^*_{q,k}\cos\theta_k \\ &= \frac{2\left(P^*_k v_{d,k} + Q^*_k v_{q,k}\right)}{v^2_{d,k} + v^2_{q,k}}\sin\theta_k + \frac{2\left(P^*_k v_{q,k} - Q^*_k v_{d,k}\right)}{v^2_{d,k} + v^2_{q,k}}\cos\theta_k \end{aligned} \tag{6}$$

where P_k^* and Q_k^* are active and reactive power references, respectively.

C. Cost Function

The MPC multi-objective cost function g compares voltage and current step ahead estimations to their references for all possible switching states. At each time step, the switching state that minimizes the cost function is selected. In the proposed control scheme, current and voltage control variables, λ_i and λ_v, are used to select the mode of operation. The cost function subject to minimization is given by,

$$g = \lambda_i \left| i_{2,k}^* - i_{2,k+1} \right| + \lambda_v \left| v_{o,k}^* - v_{o,k+1} \right| \quad (7)$$

where the voltage reference $v_{o,k}^*$ is either generated from an internal lookup table or, in the case of synchronization, is a target voltage waveform.

III. Rank-Based Control Strategy

Fig. 1 depicts the proposed controller structure. A grid-forming/following approach is implemented in the proposed controller where exactly one VSC in an islanded system operates in voltage-control mode and behaves as the central point of synchronization. If grid-tied, all VSCs operate in current-control mode and follow the utility grid's waveform. The VSC(s) at a PCC to the utility grid behaves as a central point of synchronization.

The operational mode of each VSC is determined by its rank R and the ranks of neighboring, tied VSCs. Ranks are conveyed between neighboring VSCs and are the only pieces of information shared between buses via the sparse communication layer. Each VSC begins with a unique integer ID to differentiate it from other VSCs in the system and create a predefined control structure within an islanded microgrid. Considering the i^{th} VSC, a constant, unique initial rank $R_{o,i}$ is then derived using,

$$R_{o,i} = (ID)_i \times N \quad (8)$$

where N is the maximum number of total VSCs within the microgrid. The application of (8) ensures at least N-1 integer ranks between VSC_i and any tied neighbor. The final rank of VSC_i, R_i, is dependent on the initial rank $R_{o,i}$, the binary state of the utility tie to the i^{th} local bus G_i, and the ranks of n neighboring, tied VSCs. The rank R_i at time step k is given by,

$$R_{i,k} = G_{i,k} + \min_{j=0:n} \left[T_{ij,k} \left(B_{j,k-1} + 1 \right) + R_{o,i} \left(1 - T_{ij,k} \right) \right] \left(1 - G_{i,k} \right) \quad (9)$$

where T_{ij} is the binary tie command for a line between buses i and j, and B_j is the rank of the j^{th} VSC. The rank assignment process is further explained by Algorithm 1.

A comparison of VSC_i's rank R_i to the ranks of its neighbors determines its operational mode. If R_i is less than the ranks of neighboring, tied VSCs, R_i=$R_{o,i}$, and VSC_i operates in voltage-control mode. Otherwise, R_i equals the rank of VSC_i's least-ranking tied neighbor incremented by one, and VSC_i operates in current-control mode. The only exception to this rule applies to grid-tied VSCs, which are assigned the lowest possible rank of 1 and always operate in current control mode. This eliminates the possibility of a grid-tied VSC synchronizing to a different VSC within the system and ensures that the direction of synchronization at any point within a grid-tied microgrid is always toward the nearest

Algorithm: VSC ranking scheme and weight factor determination

Initialization: $B=[B_1\ B_2\ \dots\ B_M]_{1xM}$, $T=[T_1\ T_2\ \dots\ T_M]_{1xM}$, ID=ID;

1:Initial rank formulation

$R_o \leftarrow ID*N$

2:Rank assignment

If (G =*1*)
  $R \leftarrow 1$
  $\lambda_i \leftarrow 1$
  $\lambda_V \leftarrow 0$, grid-tied and current-control mode
Else
  $R \leftarrow R_o$
  $\lambda_i \leftarrow 0$
  $\lambda_V \leftarrow 1$, islanded and voltage-control mode
  For (*j = 1:M*)
    If (*T(j)==1 && B(j) < R*)
      $R \leftarrow B(j) + 1$
      $\lambda_i \leftarrow 1$
      $\lambda_V \leftarrow 0$, islanded and current-control mode
    end if
  end for
end if

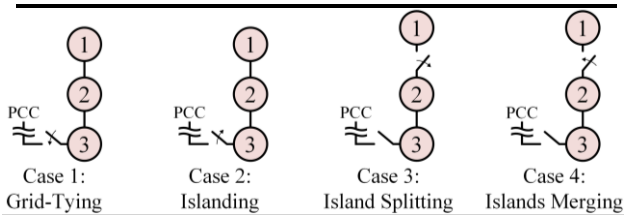

Fig. 2. Configurations for four case studies.

TABLE. I: System Specifications

Parameter	Value
DC Link Voltages V_{DC}	200V
Sampling Time T_s	20µs
Filter Inductor L_f	3mH
Filter Resistance R_f	0.03Ω
Filter Capacitance C_f	10µF
Rated Grid Voltage V_G	$95V_{pk}$
Rated Island Voltage V_o	$100V_{pk}$

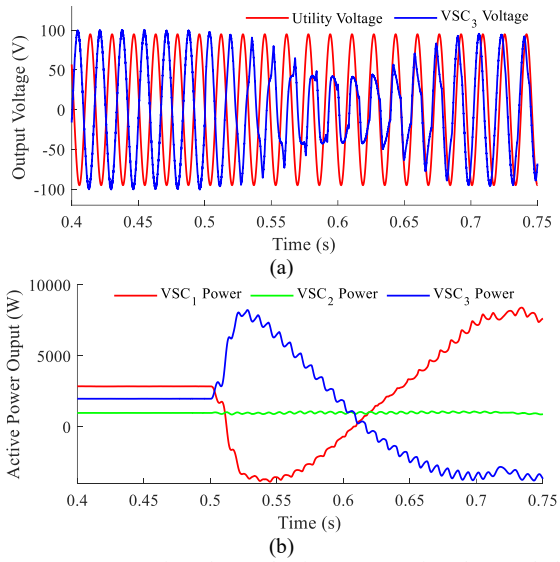

Fig. 3. Case 1a operation of non-adaptive, MPC-equipped VSCs during a grid-tie event. VSC_3 begins synchronization to the utility grid at t = 0.5 seconds. (a) Utility voltage, VSC_3 voltage. (b) VSC_1, VSC_2, VSC_3 active powers.

PCC. In this way, multiple VSCs within the microgrid can tie or untie to the same utility grid seamlessly. As the topology of the microgrid changes, ranks automatically adapt to guarantee one voltage-controlled source in an islanded system and zero voltage-controlled sources in a grid-tied system. Each VSC synchronizes to its least-ranking tied neighbor, forming a chain of connected VSCs whose ranks grow consecutively larger as lowest rank of the network's grid-forming or grid-tied VSC is propagated from one VSC to another.

If the microgrid is divided into smaller networks or the present grid-forming, voltage-controlled source is disconnected, the next lowest-ranked VSC within the system immediately transitions to voltage-controlled operation. Furthermore, the direction of synchronization in the new network is immediately and automatically updated to point toward the new grid-forming VSC. If two islanded microgrids, each with their own independent grid-forming VSC, are tied together at a single line, the lowest-ranking grid-forming VSC is selected as the voltage-controlled VSC of the combined system. Then, the rank of this voltage-controlled VSC forces a shift of synchronization directionality within the secondary microgrid as all VSCs follow the new system's voltage-controlled, grid-forming VSC.

IV. Simulation Case Studies and Results

The proposed controller and ranking scheme are implemented in MATLAB Simulink for system level simulations. Four case studies test the performance of the adaptive rank-based controller under four topology shifts in a microgrid network with three single-phase VSCs, as outlined in Fig. 2. The physical and electrical parameters of the simulated circuit are included in Table I. N, the maximum theoretical number of VSCs within the system, is set to 100.

Case 1 offers a comparison between grid-tying microgrids with and without the proposed rank-based controller. Case 1a tests the performance of simple, non-adaptive MPC-controlled VSCs operating in a microgrid throughout the grid-tying transition. VSC_1 is a fixed voltage-controlled source within the islanded microgrid, and VSC_3 is commanded to synchronize to the external utility grid at t = 0.5 seconds. Fig. 3a shows the subsequent distortion of the output voltage waveform as VSC_1 and VSC_3 operate in competing voltage-control modes. The active powers of VSC_1 and VSC_3 also destabilize, as shown in Fig. 3b.

Case 1b tests the performance of predictive VSCs with the proposed adaptive ranking scheme throughout the grid-tying transition. Fig. 4c shows the ranks of each VSC over time. Prior to t = 0.5 seconds, VSC_1 possesses the lowest rank (R_1=$R_{o,1}$=100) thus operates in voltage-control mode while VSC_2 and VSC_3 operate in current-control mode. At t = 0.5 seconds, VSC_3 is commanded to synchronize to the utility grid and its rank immediately adapts (R_3=1). VSC_3 transitions to voltage-control mode to perform the synchronization, and because of the shift in ranks, VSC_1 transitions to current-control mode. The seamless synchronization to the utility grid is completed at t = 0.65 seconds, as shown in Fig. 4a, when the line is closed in and VSC_3 returns to current-control mode.

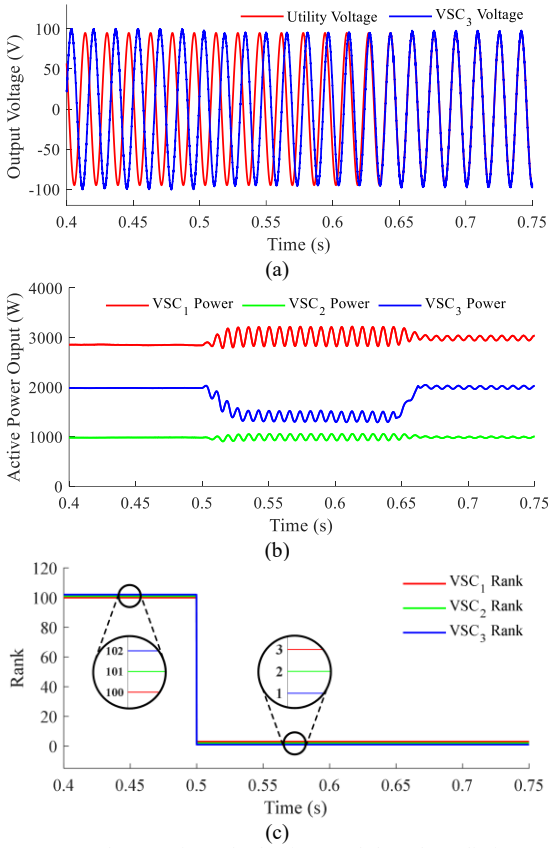

Fig. 4. Case 1b operation of adaptive, rank-based predictive VSCs during a grid-tie event. VSC_3 begins synchronization to the utility grid at t = 0.5 seconds. (a) Utility voltage, VSC_3 voltage. (b) VSC_1, VSC_2, VSC_3 active powers. (c) VSC_1, VSC_2, VSC_3 ranks.

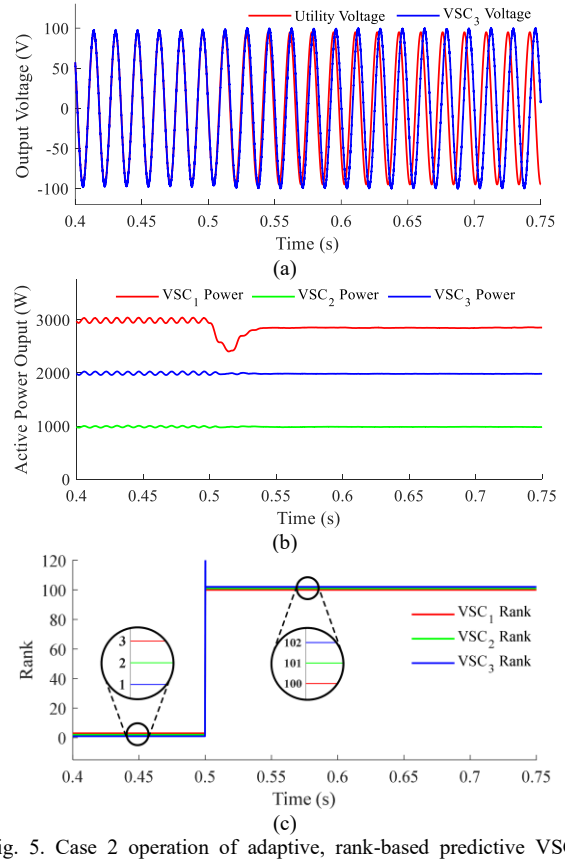

Fig. 5. Case 2 operation of adaptive, rank-based predictive VSCs during an islanding event. VSC_3 disconnects from the utility grid at t = 0.5 seconds. (a) Utility voltage, VSC_3 voltage. (b) VSC_1, VSC_2, VSC_3 active powers. (c) VSC_1, VSC_2, VSC_3 ranks.

Active power remains stable throughout the transition, as is evident from Fig. 4b.

Case 2 explores the use of ranked predictive controllers during an islanding event. Fig. 5c shows the ranks of each VSC over time. While directly grid-tied, the rank of VSC_3 (R_3=1) ensures all VSCs operate in current control mode. VSC_3 islands from the utility grid at t = 0.5 seconds and ranks increase accordingly. VSC_1's rank (R_1=$R_{o,1}$=100) is now the lowest of the islanded network, causing VSC_1 to transition to voltage-control mode while VSC_2 and VSC_3 remain in current control mode. The slight shift in voltage magnitude and frequency shown in Fig. 5a is evidence of successful islanding from the utility grid. Active power throughout the transition is shown in Fig. 5b.

Case 3 tests a dynamic topology that comprises an islanded microgrid split into two smaller grid clusters. Fig. 6c shows the ranks of each VSC over time. Prior to t = 0.5 seconds, VSC_1 possesses the lowest rank (R_1=$R_{o,1}$=100) and supports the islanded system in voltage-control. At t = 0.5 seconds, the tie line between VSC_1 and VSC_2 is opened. VSC_1 continues operating in voltage-control mode as its own, independent grid cluster. VSC_2 possesses the lowest rank (R_2=$R_{o,2}$=200) of the second grid cluster and transitions to voltage-control mode as well. Fig. 6a shows the voltage waveforms of both isolated grid clusters. An artificial frequency deviation is added to the control loop of VSC_2 to better illustrate the separation. Active power throughout the transition is shown in Fig. 6b.

Case 4 tests the reverse of Case 3, with a dynamic topology that comprises two islanded grid clusters merging into a single, larger, islanded microgrid. Fig. 7c shows the ranks of each VSC over time. The first grid cluster contains just VSC_1 operating in voltage-control mode. The second grid cluster comprises VSC_2 and VSC_3. The lower rank of VSC_2 (R_2=$R_{o,2}$=200) causes it to operate in voltage-control mode while VSC_3 meets its power reference in current-control mode. The tie line between VSC_1 and VSC_2 is commanded to close at t = 0.5 seconds. VSC_2 immediately adapts to the lower rank of VSC_1 and begins synchronizing its waveform to that of VSC_1 while VSC_3 follows. Seamless synchronization between the grid clusters is achieved at t = 0.67 seconds, as is evident in Fig. 7a, when the line between VSC_1 and VSC_2 is closed in and VSC_2 transitions to current-control mode. VSC_1 continues operating in voltage-control mode as the grid-forming source of the merged microgrid. Active power throughout the transition is shown in Fig. 7b.

V. Experimental Analysis and Results

Device level hardware experiments are conducted using Typhoon HIL and a single-phase H-bridge inverter with LC filter. The hardware testbed and Typhoon HIL 402 controller are illustrated in Fig. 8. In the following case study, the single, grid-tied VSC experiences an active power step change at t = 0.5 seconds. Fig. 9a shows the measured voltage and output current waveforms. During the step change, PCC voltage is held steady by an external utility grid and the output current smoothly rises to account for the increase in desired active power. Active and reactive

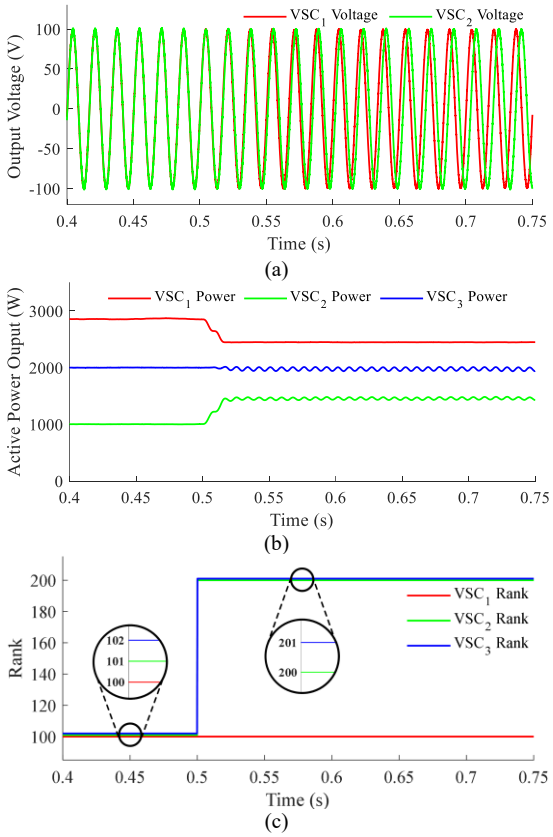

Fig. 6. Case 3 operation of adaptive, rank-based predictive VSCs during an island splitting event. Tie line connecting VSC_1 and VSC_2 opens at t = 0.5 seconds. (a) VSC_1 voltage, VSC_2 voltage. (b) VSC_1, VSC_2, VSC_3 active powers. (c) VSC_1, VSC_2, VSC_3 ranks.

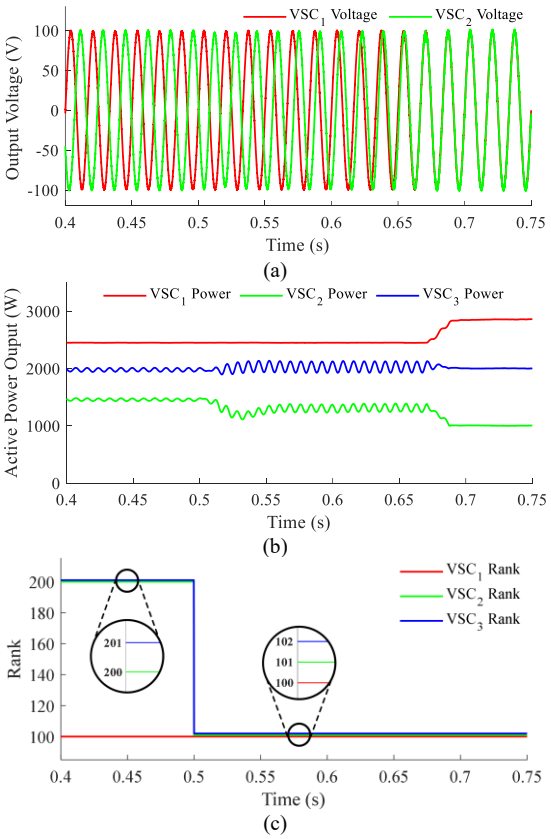

Fig. 7. Case 4 operation of adaptive, rank-based predictive VSCs during an islands merging event. VSC_2 begins synchronization to VSC_1 at 0.5 seconds. (a) VSC_1 voltage, VSC_2 voltage. (b) VSC_1, VSC_2, VSC_3 active powers. (c) VSC_1, VSC_2, VSC_3 ranks.

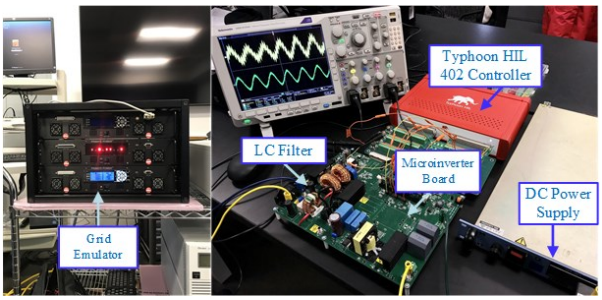

Fig. 8. Hardware testbed.

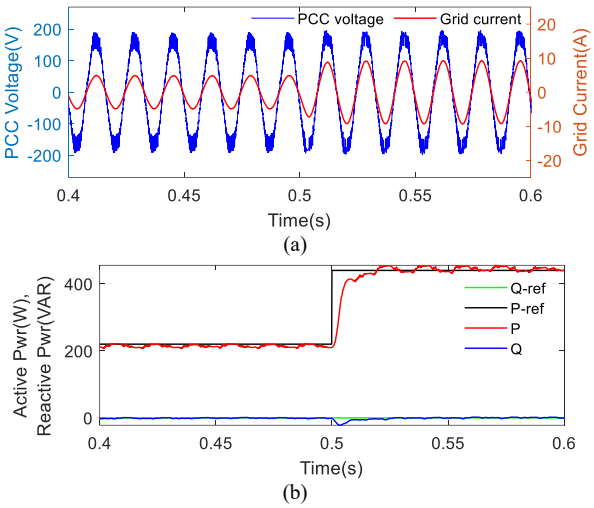

Fig. 9. Hardware experiment for evaluating the dynamic response of the proposed MPC controller – a step change in the active power reference occurs at t = 0.5 seconds.

powers, along with their respective references, are included in Fig. 9b. This study demonstrates the seamless power tracking ability of the MPC in a grid-tied configuration.

VI. Conclusion

An adaptive, rank-based MPC framework is proposed in this paper to enable full synchronization of re-configurable microgrids with adaptive boundaries and MPCC. The controller is designed to automatically adapt to topology changes within an islanded or grid-tied network for the purposes of synchronization and operational mode assignment. Via simulation case studies, the presented controller is demonstrated to increase a grid cluster's resiliency and flexibility in the event of changing topologies. Performance of the single-phase VSC design is further verified by a hardware analysis.

Acknowledgment

This work was supported by the U.S. National Science Foundation under Grant ECCS-2033956.

Reference

[1] Z. Li, M. Shahidehpour, F. Aminifar, A. Alabdulwahab, and Y. Al-Turki, "Networked microgrids for enhancing the power system resilience," *Proceedings of the IEEE,* vol. 105, no. 7, pp. 1289-1310, 2017.

[2] S. Parhizi, H. Lotfi, A. Khodaei, and S. Bahramirad, "State of the art in research on microgrids: A review," *Ieee Access,* vol. 3, pp. 890-925, 2015.

[3] A. Khan, M. Hosseinzadehtaher, M. B. Shadmand, S. Bayhan, and H. Abu-Rub, "On the Stability of the Power Electronics-Dominated Grid: A New Energy Paradigm," *IEEE Industrial Electronics Magazine,* vol. 14, no. 4, pp. 65-78, 2020.

[4] D. T. Ton and M. A. Smith, "The US department of energy's microgrid initiative," *The Electricity Journal,* vol. 25, no. 8, pp. 84-94, 2012.

[5] O. H. Abu-Rub, A. Y. Fard, M. F. Umar, M. Hosseinzadehtaher, and M. B. Shadmands, "Towards Intelligent Power Electronics-Dominated Grid via Machine Learning Techniques," *IEEE Power Electronics Magazine,* vol. 8, no. 1, pp. 28-38, 2021.

[6] S. D. silva, M. Shadmand, S. Bayhan, and H. Abu-Rub, "Towards Grid of Microgrids: Seamless Transition between Grid-Connected and Islanded Modes of Operation," *IEEE Open Journal of the Industrial Electronics Society,* vol. 1, pp. 66-81, 2020.

[7] D. Zhang, "Operation of microgrid at constant frequency with a standby backup grid-forming generator," in *2016 IEEE International Conference on Power System Technology (POWERCON)*, 2016: IEEE, pp. 1-6.

[8] X. Li, H. Zhang, M. B. Shadmand, and R. S. Balog, "Model Predictive Control of a Voltage-Source Inverter With Seamless Transition Between Islanded and Grid-Connected Operations," *IEEE Transactions on Industrial Electronics,* vol. 64, no. 10, pp. 7906-7918, 2017.

[9] J. W. Simpson-Porco, Q. Shafiee, F. Dörfler, J. C. Vasquez, J. M. Guerrero, and F. Bullo, "Secondary frequency and voltage control of islanded microgrids via distributed averaging," *IEEE Transactions on Industrial Electronics,* vol. 62, no. 11, pp. 7025-7038, 2015.

[10] S. Shah, H. Sun, D. Nikovski, and J. Zhang, "Consensus-based synchronization of microgrids at multiple points of interconnection," in *2018 IEEE Power & Energy Society General Meeting (PESGM)*, 2018: IEEE, pp. 1-5.

[11] A. Y. Fard and M. B. Shadmand, "Multitimescale Three-Tiered Voltage Control Framework for Dispersed Smart Inverters at the Grid Edge," *IEEE Transactions on Industry Applications,* vol. 57, no. 1, pp. 824-834, 2021.

[12] M. Easley, M. B. Shadmand, and H. Abu-Rub, "Hierarchical Model Predictive Control of Grid-Connected Cascaded Multilevel Inverter," *IEEE Journal of Emerging and Selected Topics in Power Electronics,* pp. 1-1, 2020.

[13] M. Hosseinzadehtaher, A. Khan, M. Easley, M. B. Shadmand, and P. Fajri, "Self-healing Predictive Control of Battery System in Naval Power System with Pulsed Power Loads," *IEEE Transactions on Energy Conversion,* pp. 1-1, 2020.

[14] M. Easley, S. Jain, M. Shadmand, and H. Abu-Rub, "Autonomous Model Predictive Controlled Smart Inverter With Proactive Grid Fault Ride-Through Capability," *IEEE Transactions on Energy Conversion,* vol. 35, no. 4, pp. 1825-1836, 2020.

[15] M. B. Shadmand, S. Jain, and R. S. Balog, "Autotuning Technique for the Cost Function Weight Factors in Model Predictive Control for Power Electronic Interfaces," *IEEE Journal of Emerging and Selected Topics in Power Electronics,* vol. 7, no. 2, pp. 1408-1420, 2019.

[16] N. Panten, N. Hoffmann, and F. W. Fuchs, "Finite control set model predictive current control for grid-connected voltage-source converters with LCL filters: A study based on different state feedbacks," *IEEE Transactions on Power Electronics,* vol. 31, no. 7, pp. 5189-5200, 2015.